WESTERN REGION TECHNICAL ATTACHMENT
NO. 97-03
JANUARY 21, 1997

WHY IS HIGH RESOLUTION IMPORTANT IN THE WEST? AN EARLY LOOK AT THE ETA-10 MODEL OUTPUT

Mike Staudenmaier, Jr. - WRH-SSD/NWSFO Salt Lake City, UT

Introduction

The Eta-29 model has proven to be a valuable model in the forecasting process due to its high resolution and model physics (Burks and Staudenmaier, 1996; Janish and Weiss, 1996; Schneider et al., 1996). A higher resolution nest of the Eta-29 model, at 10 km resolution, is currently being run at NCEP with the Western Region participating in an evaluation of its skill. This Technical Attachment will look at some early results from the model, based on a rerun of the 11-12 December 1995 'Storm of the Decade', showing that the increased resolution has led to some better forecasts with details previously unavailable from the NCEP model suite.

Model Description

The Eta-10 model has the same physical package as the Eta-29 model as explained by Staudenmaier (1996). Currently, the only differences in the model are in model resolution, both in the vertical and in the horizontal, domain size, and the initialization scheme. The Eta-10 model currently has 60 vertical levels, as opposed to 50 in the Eta-29. Many of these levels are below 900 mb, a feature designed mainly for the Atlanta Olympics, where the Eta-10 was first run. Thus, the main impact of these additional levels will be seen only near the coast. The domain size of the Eta-10, is smaller than the Eta-29, as seen in Figure 1. The Eta-10 model is currently initialized off the 0900 UTC Eta-29 grid, using a three-dimensional variational analysis technique (3DVAR). The 3DVAR will likely be more flexible than the Optimum Interpolation (OI) scheme currently used in the Eta-29 model, and will make it possible to use many new data sources and utilize existing data better. For more information regarding 3DVAR see Staudenmaier (1996).

Examples of Output

This section will examine various meteorological fields centered near the 1200 UTC period on 12 December 1995. Readers wishing more background of this storm should see Burks and Staudenmaier (1996).

Washington

Figure 2 shows the model terrain over much of Washington. Many features, previously unresolvable by the models, can now be seen. Of note is Mount Olympus in the upper-left hand corner, and Mount Rainier near the bottom center portion of the diagram. Previously, none of these mountains were resolvable, even at 29 km resolution.

Figure 3 is a diagram of 500 mb relative humidity (shaded values over 70%), and omega (solid lines indicating rising motion). Clearly, a couplet of rising motion on the southern side of Mount Rainier and sinking motion on the northern side can be seen. Higher relative humidity, likely from rising motion, due to its isolated manner, is apparent on the southern flank of the mountain. The wind flow over most of Washington at this time was from around 195 degrees and quite strong. To the northwest, over Mount Olympus a similar pattern can be seen, although not quite as dramatic.

This amount of detail should allow forecasters to begin to see higher rainfall amounts in certain river basins and on isolated mountain sides. Figure 4 shows three-hour total precipitation ending at 1500 UTC 12 December, where a bulls-eye of between 1.25 and 1.50 inches of precipitation can be seen on the southern slope of Mount Rainier, with a rain shadow of less than 0.10 inches to the north.

Figure 6 shows the mean sea level pressure for the same time period. Of note is the packing of isobars on the southern flank of the mountains, including Mount Rainier. This tightening of the pressure gradient can lead to stronger winds, and even low-level jets along the sides of certain mountain ranges under certain synoptic conditions. Figure 7, indicating the lowest-level winds (and model terrain), shows the stronger winds (greater than 50 kt) along the slopes of Mount Rainier. The synoptic flow then can be seen on the plateau to the east of Mount Rainier with wind speeds of only 30 kt. Also, note the winds flowing out of the Puget Sound area and around the southern side of Mount Olympus and eventually to the Pacific Ocean.

Oregon

Figure 8 shows the lowest-level winds and model terrain over the northern portion of Oregon, through the Columbia River Gorge. Again, before the Eta-10 model, this topographical feature was poorly represented by the NCEP models. Clearly, the stronger easterly flow in the Columbia River Gorge can be seen, strengthening as it moves through the gap in the Cascades. It is likely that these winds are not forecast as strong as what occurred at that time, but for the first time, the model can begin to give an idea of where the strongest winds will occur. Also of note, is the low-level diffluence pattern seen as the winds leave the Columbia River Gorge and move toward the Pacific Ocean.

Figure 9 is a diagram of 850 mb isotachs and winds. Of note is the strong low-level coastal jet which has formed parallel to the coast. Wind speeds in the center of this jet were forecast to be near 90 kt, with further strengthening as the low pressure system intensified farther offshore. The Eta-29 model also had a defined coastal jet along the Oregon coast, but did not have as much of the detail and structure that can be seen here. The Eta-10 had more detail in the wind field through some canyons and valleys in the interior portion of Oregon, not seen in the Eta-29 model.

California

Figure 10 is a map of model terrain over portions of northern California. For the first time, the Coastal Range Mountains are clearly visible, with a well-defined Sacramento Valley. Also evident is a much smaller inlet between the Coastal Mountains into the Central Valley to the northeast of San Francisco Bay. This higher resolution of terrain should make better wind and precipitation forecasts through this portion of the state and throughout the Central Valley, as this inlet is the primary passage through which marine air enters the Central Valley.

Figure 11 is a map of mean sea level pressure over the northern portion of California. Mesoscale detail can be seen in the ridge-trough pattern located over the Coastal Range Mountains and the Sierra Nevada Mountains. The Eta-29 model developed a ridge-trough pattern over the Sierra Nevada Mountains, but never developed much over the Coastal Range Mountains due to the fact they barely existed in that model's terrain. In the Eta-10 model, the mesoscale detail clearly stands out. This has direct bearing on low-level winds over California as these mesoscale pressure patterns lead to stronger, southeasterly flow near the surface in the Sacramento Valley, and strong convergence on the western side of the valley, where locally heavy rainfall can be a result. Additionally, the development of a southerly barrier jet along the western side of the Sierra Nevada Mountains is based on the development of high pressure along the western flanks of the mountains. With the Eta-10 model, this development can be clearly seen. Thus, now that these mesoscale pressure patterns are modeled correctly, forecasters should begin seeing an improvement in wind structures over their areas of concern. Also of note is the mesoscale area of high pressure that forms to the south of Mount Shasta in the top portion of the figure. Again, higher resolution is able to capture this feature.

Figure 12 is a map of the lowest-level wind field over the same domain. As mentioned above, southeasterly winds are clearly evident over the Sacramento Valley impinging on the eastern flanks of the Coastal Range Mountains. Stronger southerly winds can be seen in the foothills of the Sierra Nevada Mountains, likely evidence of the influence of the southerly barrier jet. Farther up the slopes of the Sierra Nevada Mountains, the southwesterly flow can be seen above 5000 ft, causing tremendous convergence and heavy rainfall. Vertical motions of over 60 microbars/sec were forecast over some of the steeper terrain (not shown). However, one feature that was not captured by the models

was the near hurricane force winds that were located at the northern end of the Sacramento Valley. These strong winds occur due to the convergence of flow at the north end of the valley and flow through narrowing canyons and mountain valleys. This narrowing is likely still not resolvable at 10 km, and this is likely the reason for the model not capturing this feature.

Figure 13 is a map of three-hour accumulated precipitation in the Eta-10 model over the same domain. Many small maxima can be seen in the field, which were not visible at the lower resolution model runs. Of special note are the maxima just south of Mount Shasta near the top of the page, in the northern Sierra Nevada Mountains, and in the Coastal Range Mountains. Figure 14 is a map of the six-hour accumulated precipitation which fell on that day, ending at the same time period. Note how many of the maxima line up very close to where the heaviest precipitation fell. This clearly shows the benefits of high resolution models in regard to the generation of QPF values. Specific river basins can now be forecasted for, based on the first guess of the Eta-10 model. Interestingly, as most research has shown that models tend to underforecast heavy rainfall amounts, in this case, the Eta-10 overestimated the heavier areas of rainfall. Perhaps this suggests that the model resolution has now reached a point where the underforecasting of precipitation amounts due to orographic effects is now not so much of an issue. More verification will be needed to determine if this is true.

Conclusions

These few examples demonstrate the potential of a higher resolution model in the Western Region. Clearly, the 10 km resolution of the Eta-10 model is now capable of capturing events caused or affected by topographical forcing in a much more realistic light. With the Western Region participating in a field evaluation of this model, more events such as these will be documented, underscoring the need for an operational version of this model in the West.

Acknowledgments

The author thanks NCEP for allowing Western Region the opportunity to see model output at 10 km resolution.

References

Burks, J.E., and M.J. Staudenmaier, 1996: A comparison of the Eta and the Meso Eta models during the 11-12 December 1995 storm of the decade. *WR-Technical Attachment* **96-21.**

Janish, P.R., and S.J. Weiss, 1996: Evaluation of various mesoscale phenomena associated with severe convection during VORTEX-95 using the Meso Eta model. *Preprints, 15th Conf. on Weather Analysis and Forecasting,* AMS, Norfolk, VA. Aug, 1996.

Schneider, R.S., N.W. Junker, M.T. Eckert, and T.M. Considine, 1996: The performance of the 29 km Meso Eta model in support of forecasting at the Hydrometeorological Prediction Center. *Preprints, 15th Conf. on Weather Analysis and Forecasting,* AMS, Norfolk, VA. Aug, 1996.

Staudenmaier, M.J., 1996: A description of the Meso Eta model. *WR-Technical Attachment* **96-06**.

Staudenmaier, M.J., 1996: The initialization procedure in the Meso Eta model. *WR-Technical Attachment* **96-30**.

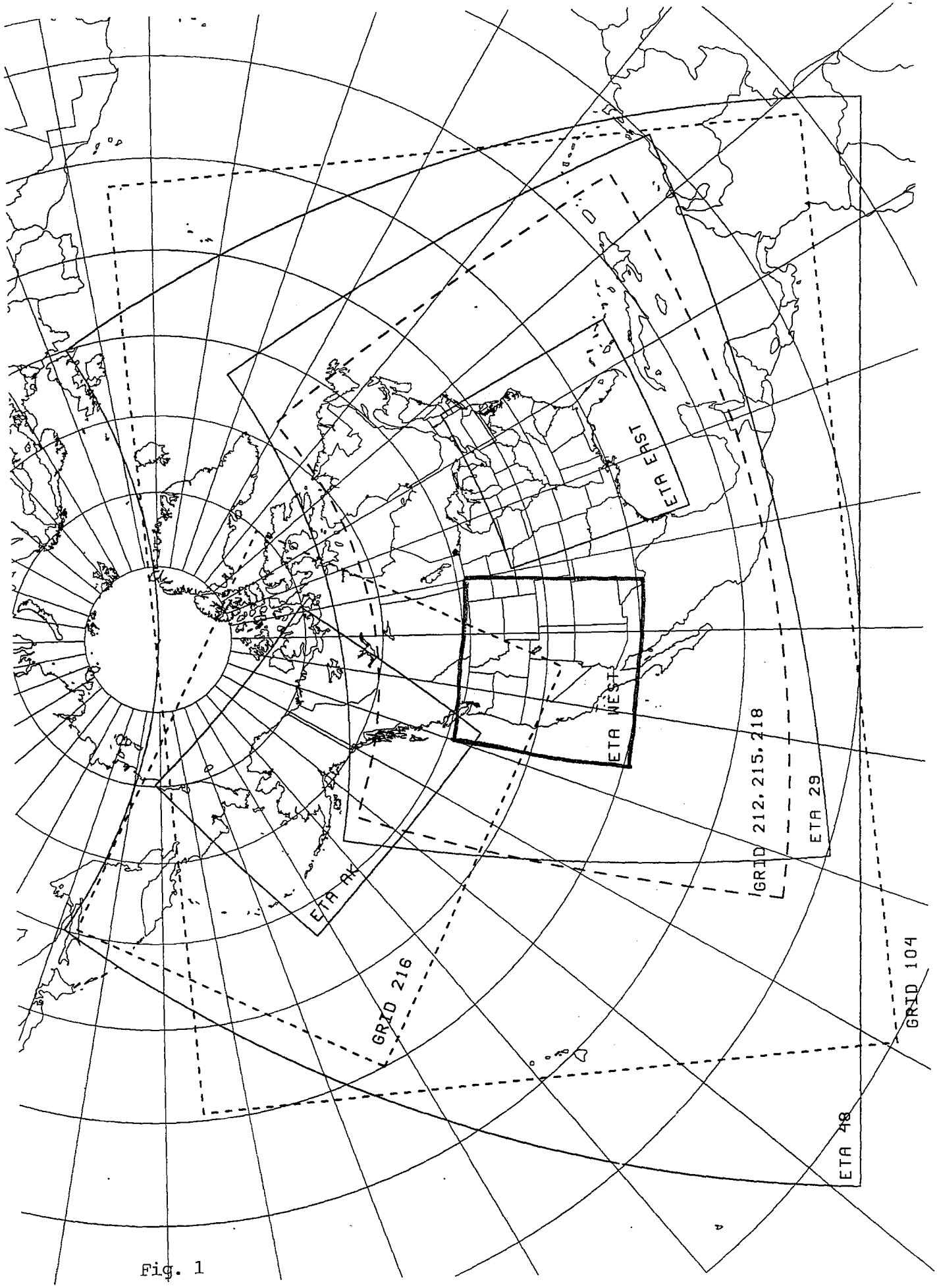
ETA EAST
ETA WEST
GRID 212, 215, 218
ETA 29
ETA AK
GRID 216
GRID 104
ETA 48

Fig. 1

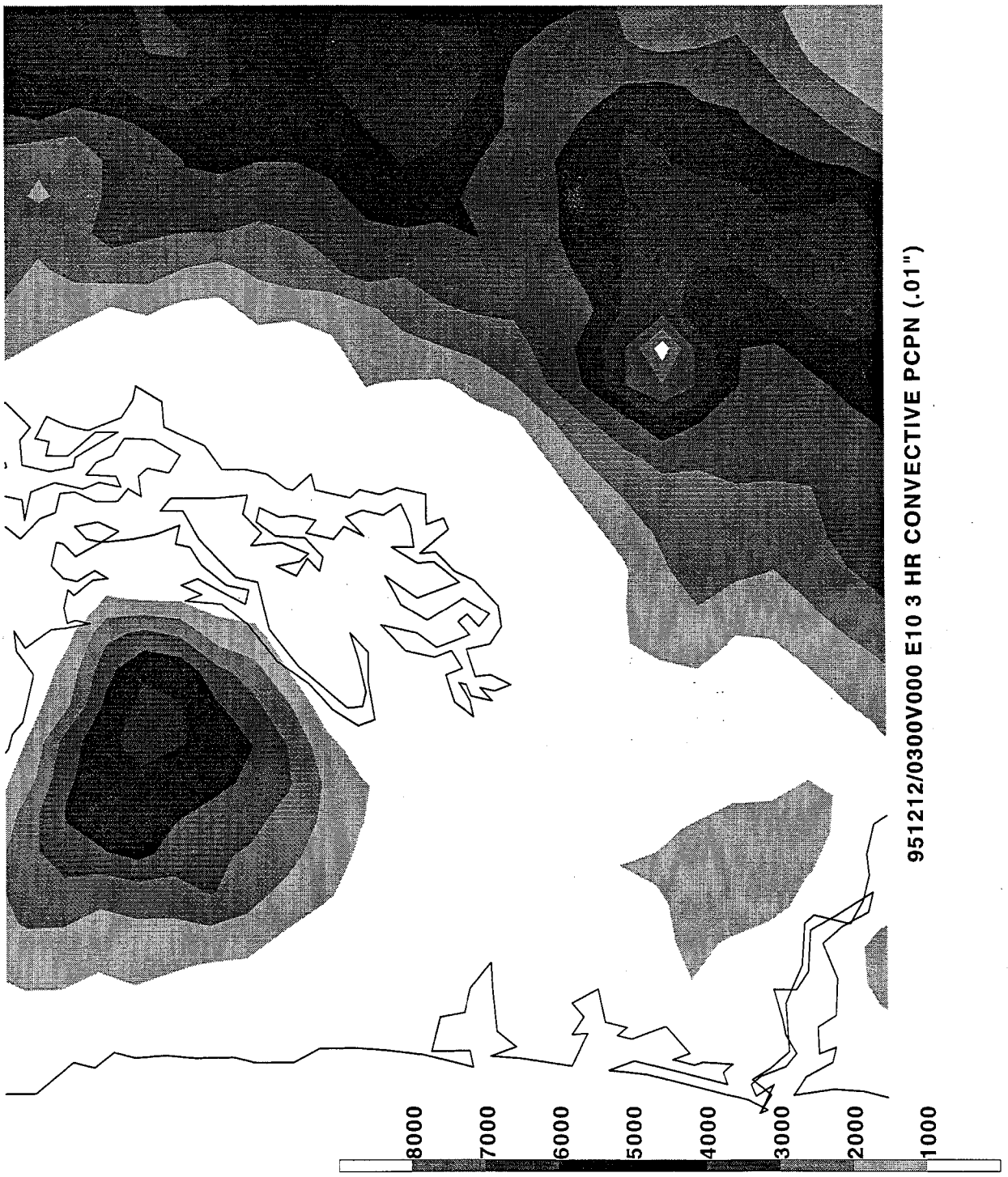
951212/0300V000 E10 3 HR CONVECTIVE PCPN (.01")
8000
7000
6000
5000
4000
3000
2000
1000

Fig. 2

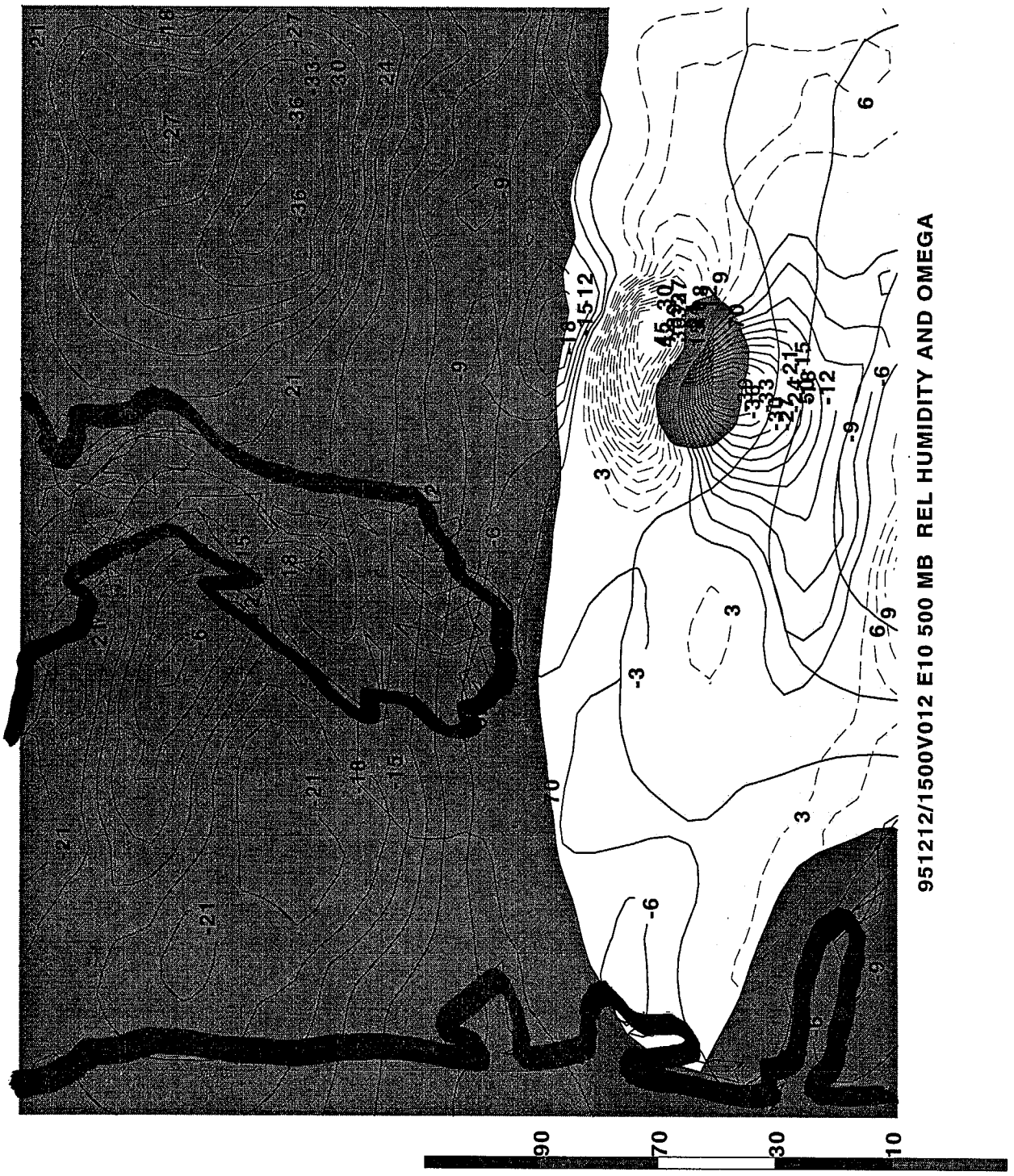

Fig. 3

Fig. 4

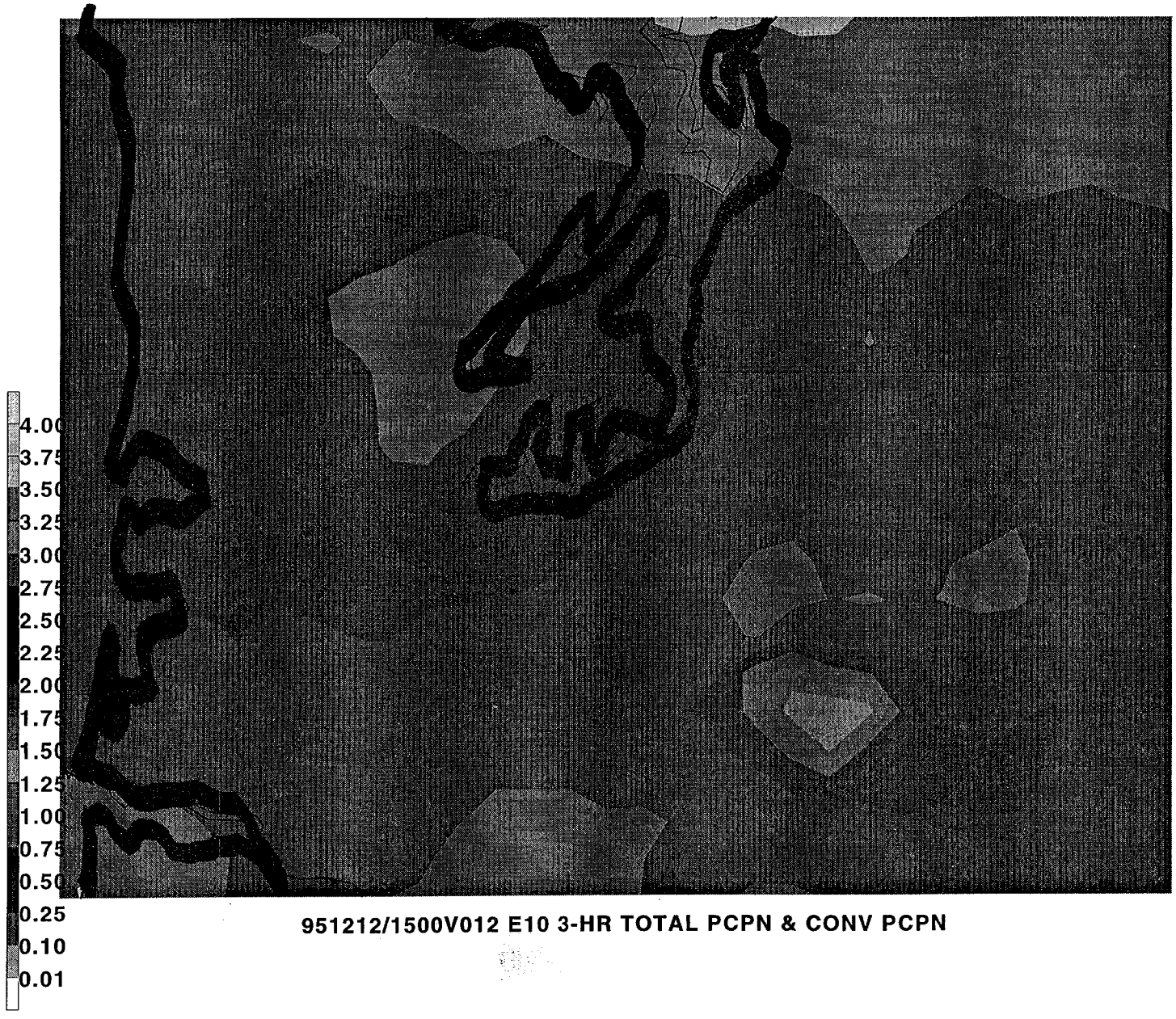
4.00
3.75
3.50
3.25
3.00
2.75
2.50
2.25
2.00
1.75
1.50
1.25
1.00
0.75
0.50
0.25
0.10
0.01
951212/1500V012 E10 3-HR TOTAL PCPN & CONV PCPN

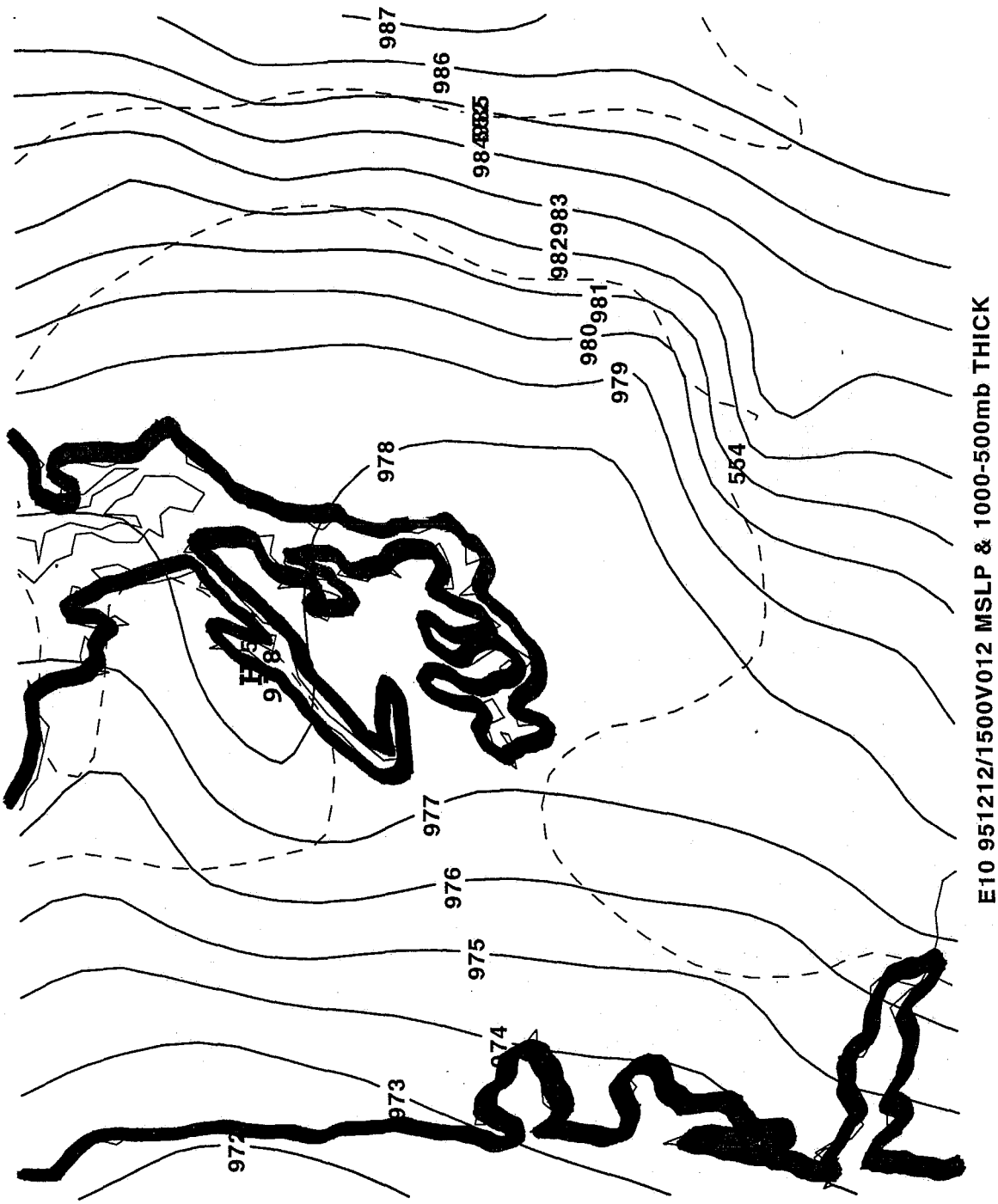
E10 951212/1500V012 MSLP & 1000-500mb THICK
987
986
984
982
983
981
980
979
978
977
976
975
974
973
972
554

Fig. 5

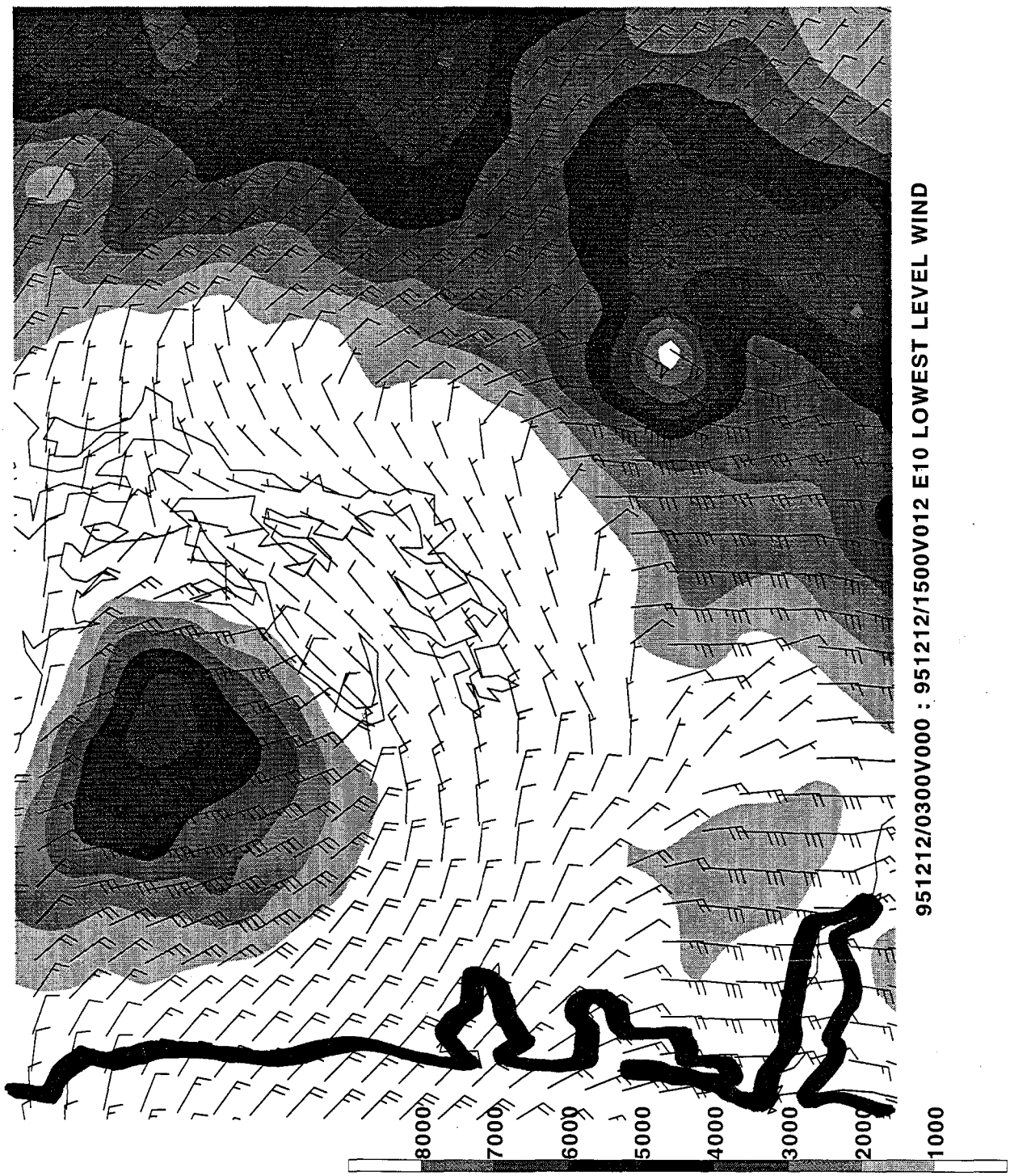
951212/0300V000 : 951212/1500V012 E10 LOWEST LEVEL WIND
8000
7000
6000
5000
4000
3000
2000
1000

Fig. 6

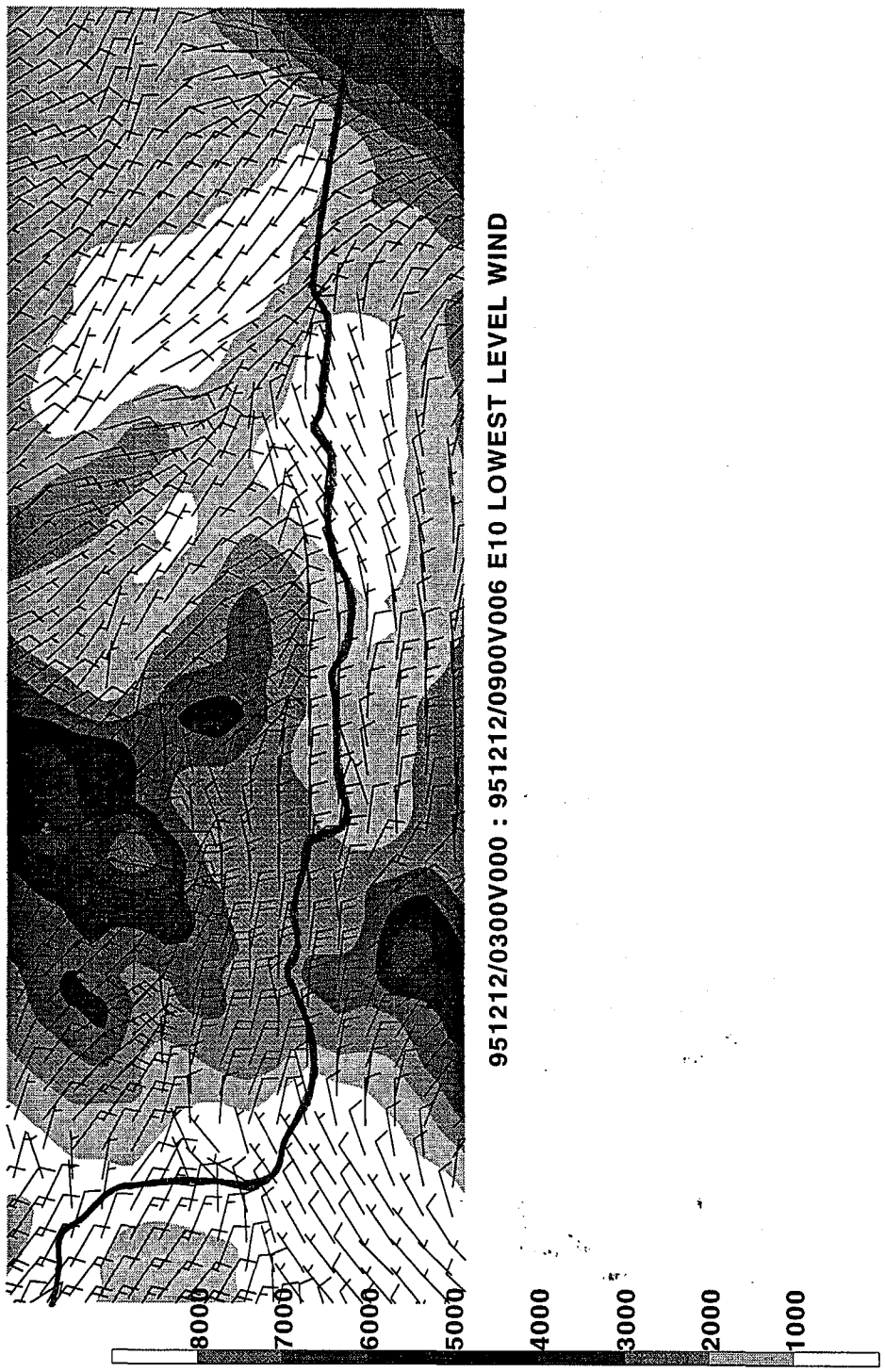
951212/0300V000 : 951212/0900V006 E10 LOWEST LEVEL WIND
8000
7000
6000
5000
4000
3000
2000
1000

Fig. 7

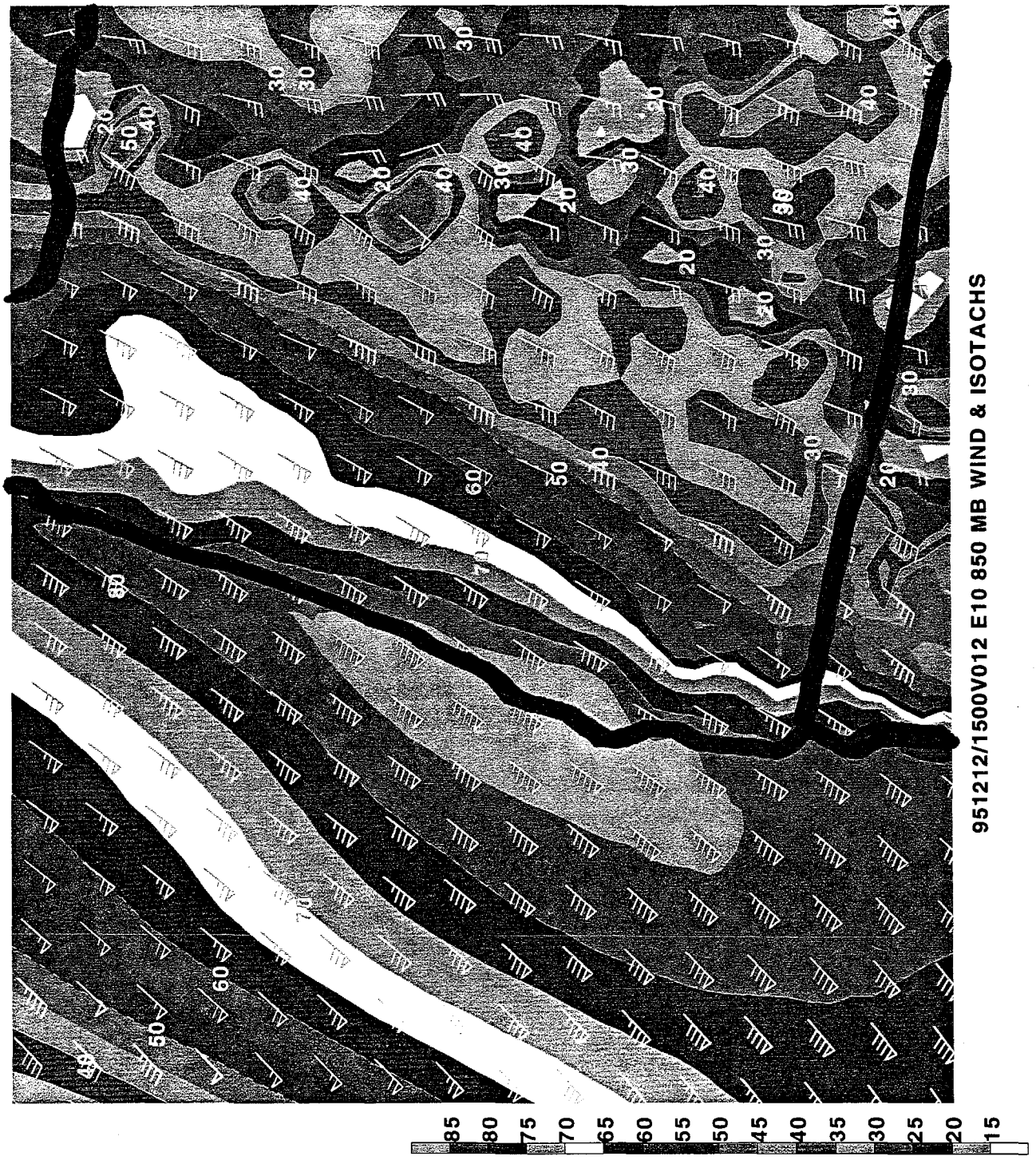
951212/1500V012 E10 850 MB WIND & ISOTACHS
85
80
75
70
65
60
55
50
45
40
35
30
25
20
15

Fig. 8

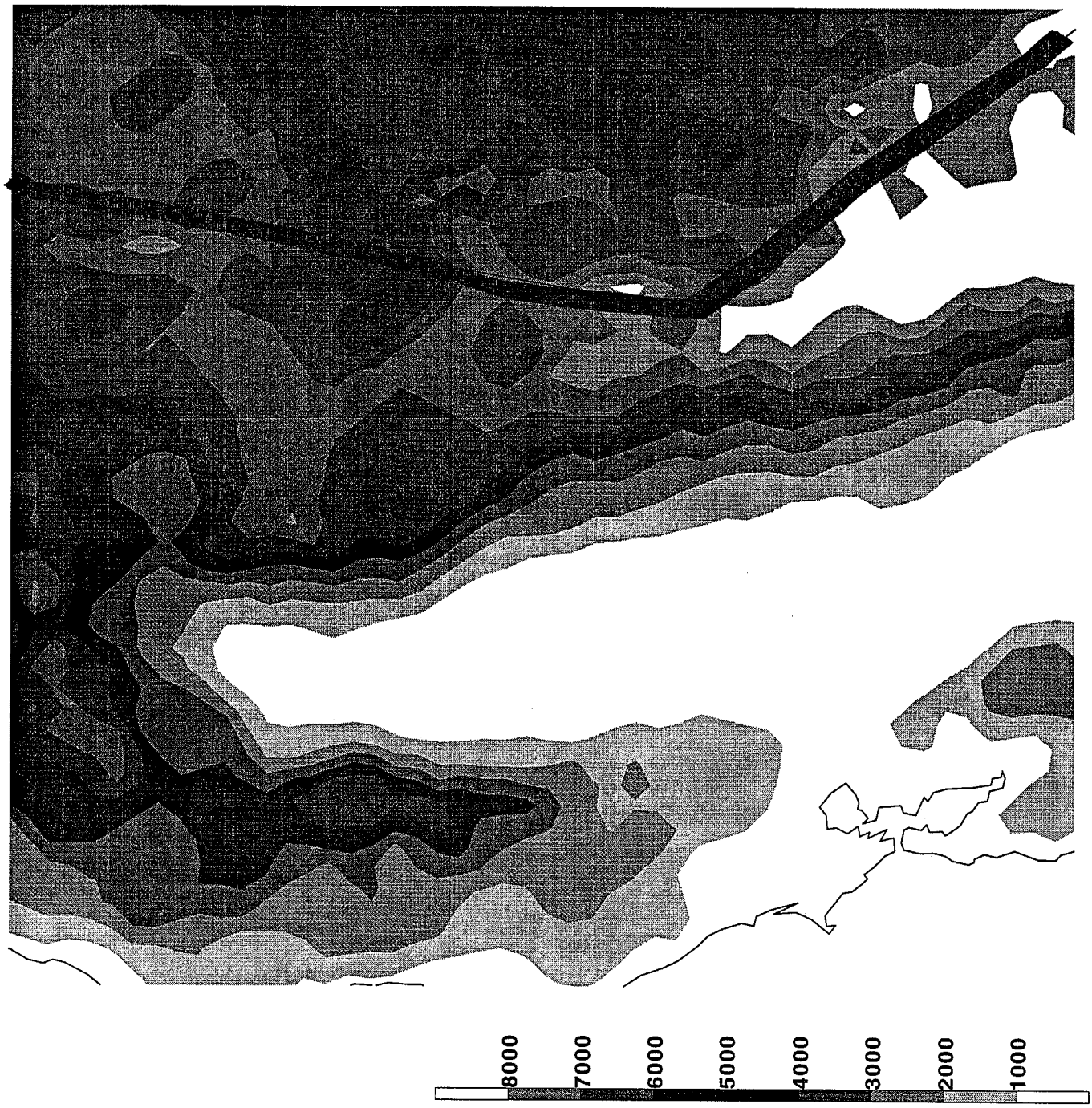
951212/0300V000 E10 3 HR CONVECTIVE PCPN (.01")
8000
7000
6000
5000
4000
3000
2000
1000

Fig. 9

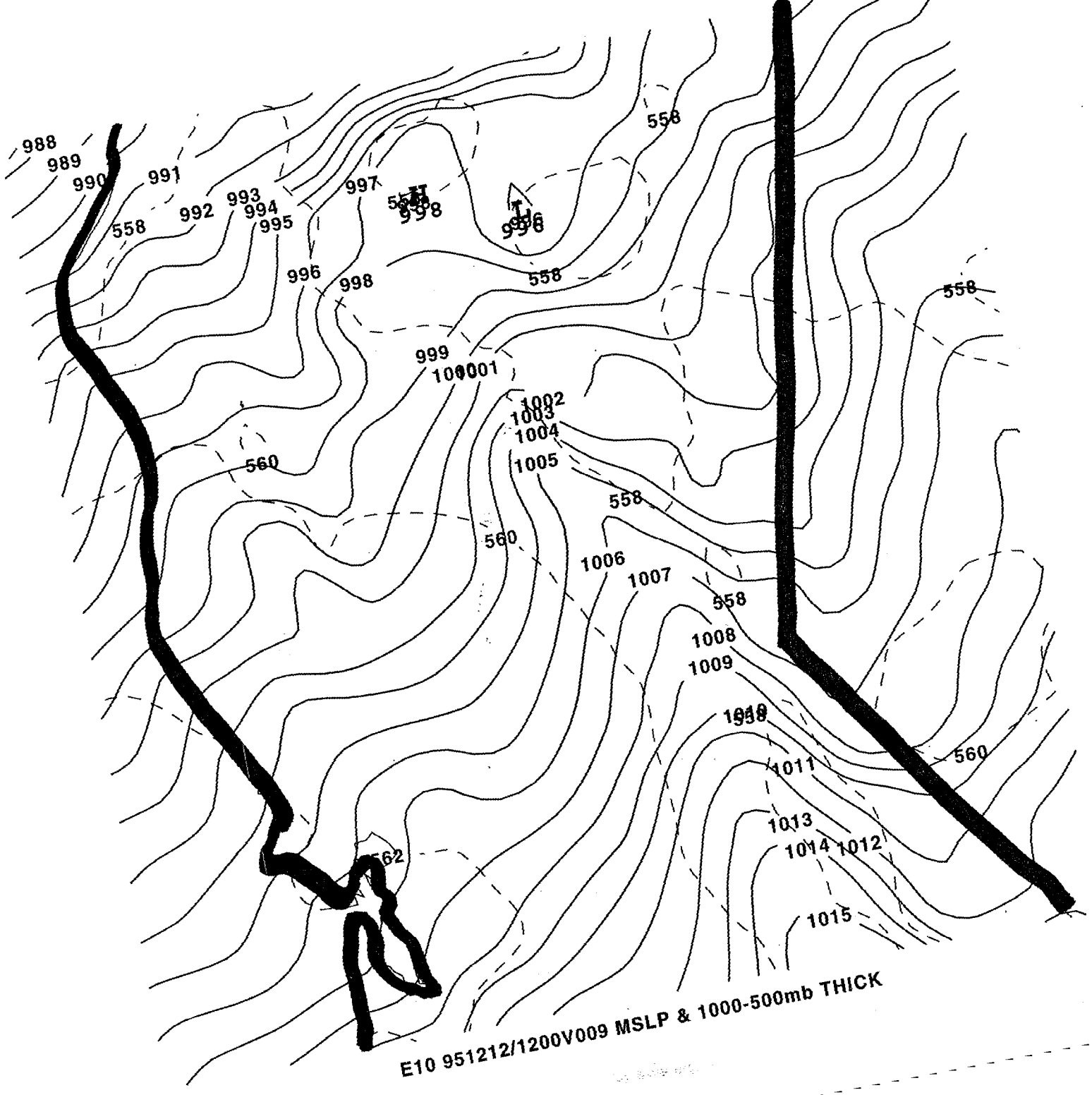
988
989
990
991
992
993
994
995
996
997
998
999
1000
1001
1002
1003
1004
1005
1006
1007
1008
1009
1010
1011
1012
1013
1014
1015
558
560
562
H
L
E10 951212/1200V009 MSLP & 1000-500mb THICK

Fig. 10

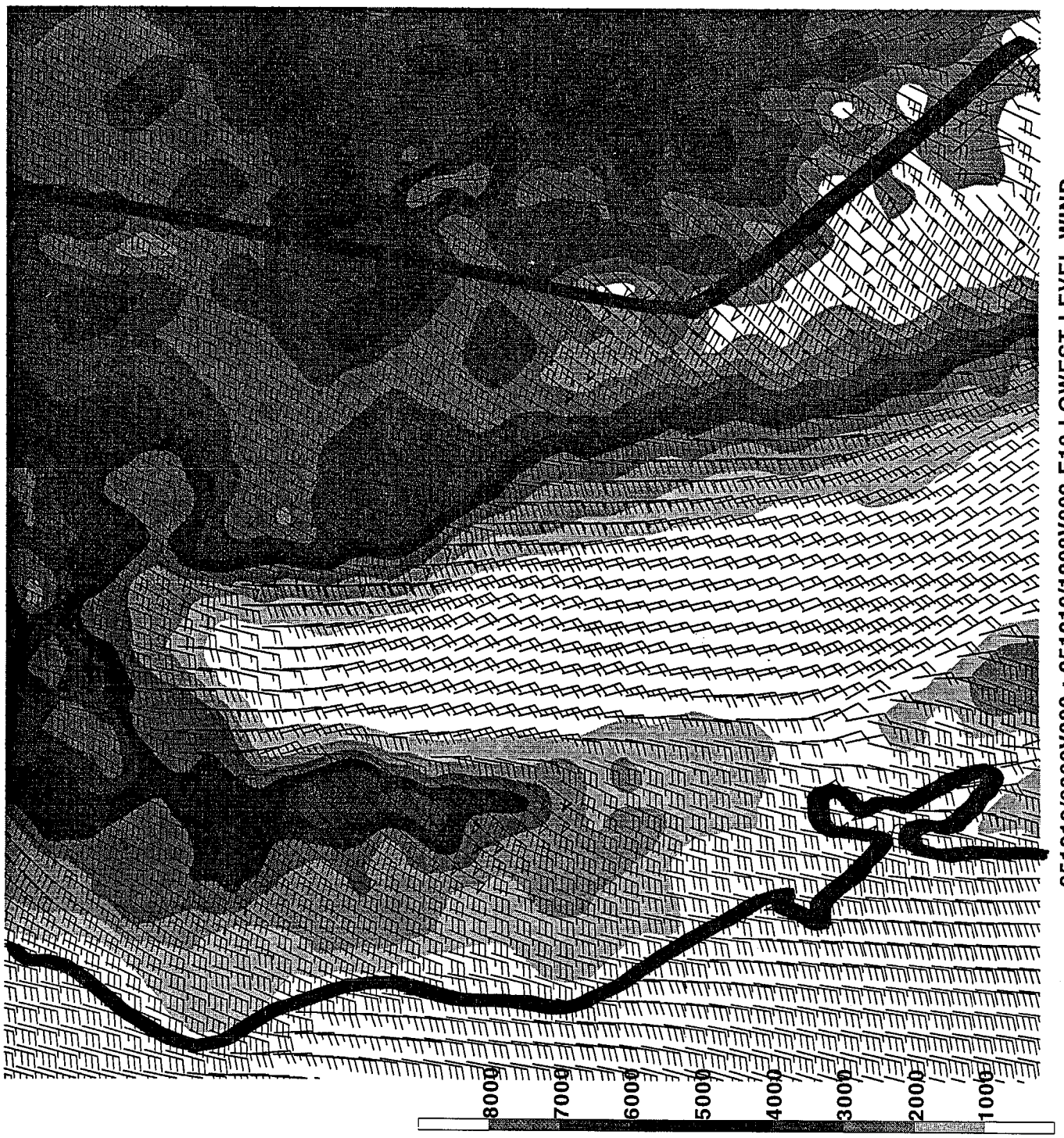
951212/0300V000 : 951212/1200V009 E10 LOWEST LEVEL WIND
8000
7000
6000
5000
4000
3000
2000
1000

Fig. 11

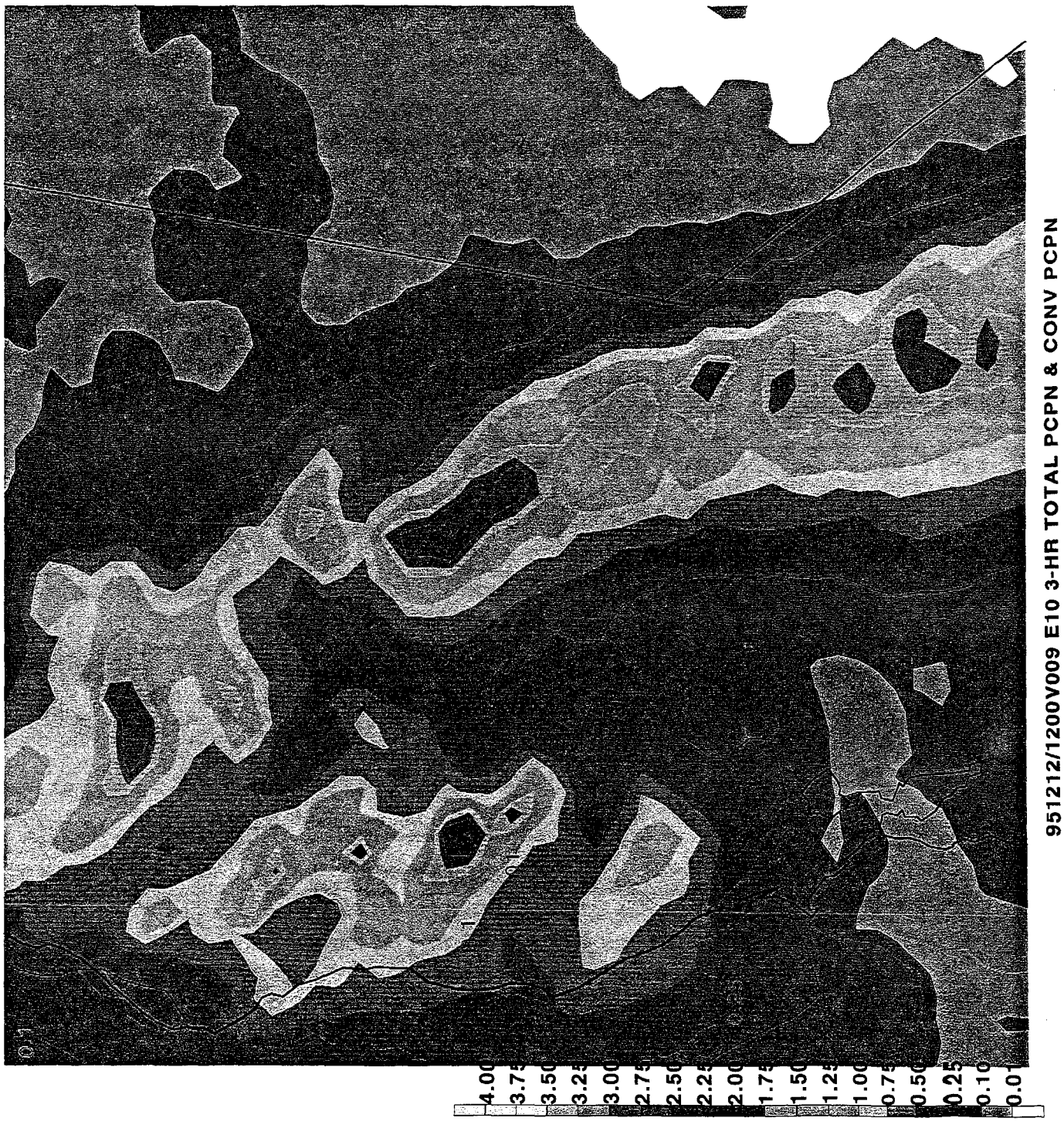
951212/1200V009 E10 3-HR TOTAL PCPN & CONV PCPN
4.00
3.75
3.50
3.25
3.00
2.75
2.50
2.25
2.00
1.75
1.50
1.25
1.00
0.75
0.50
0.25
0.10
0.01

Fig. 12

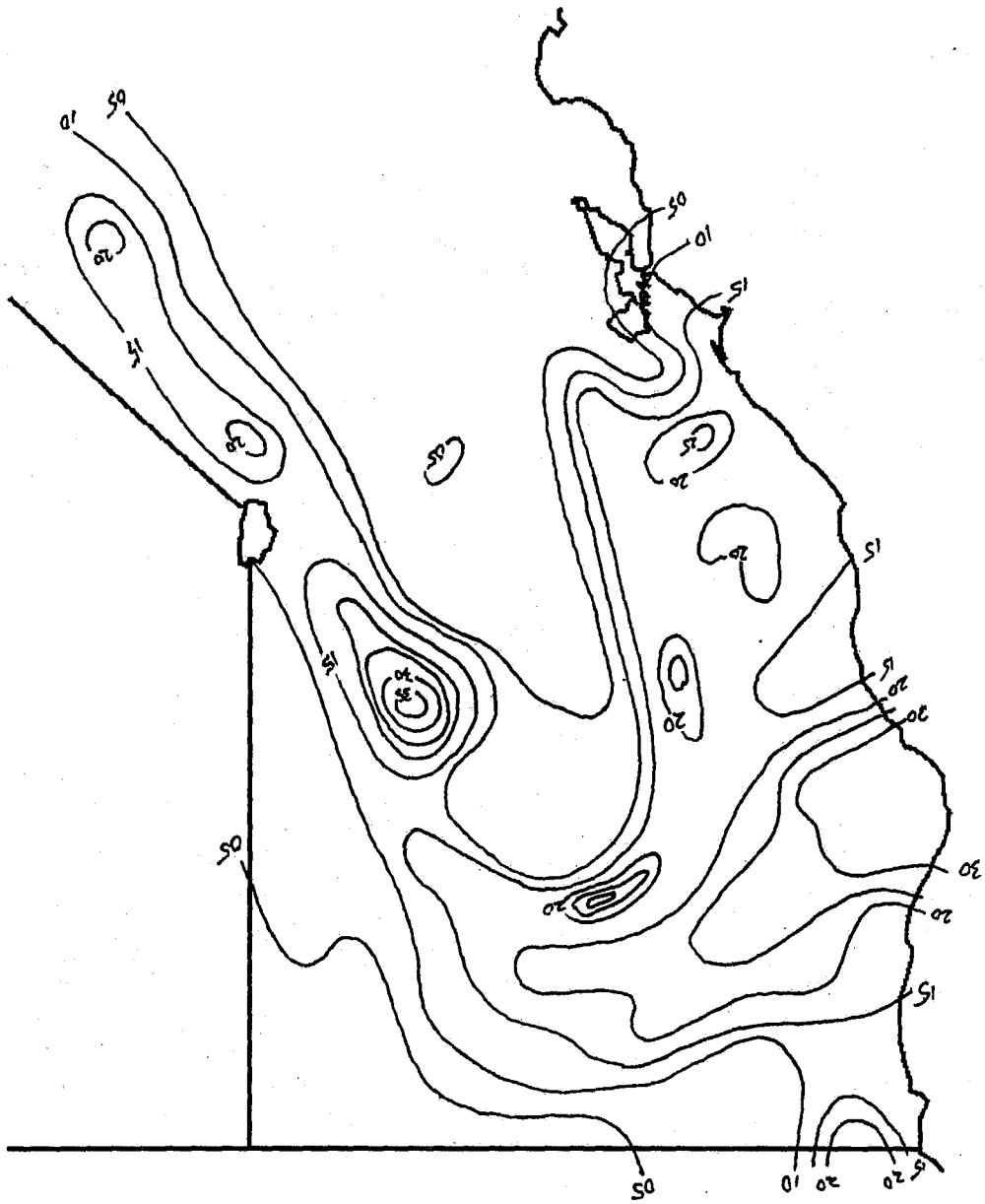

Fig. 13